Jiali Jiang*, Bachtiar Erik Valentine, Jianxiong Lu and Peter Niemz

Time dependence of the orthotropic compression Young's moduli and Poisson's ratios of Chinese fir wood

DOI 10.1515/hf-2016-0001
Received January 3, 2016; accepted April 28, 2016; previously published online May 26, 2016

Abstract: The time dependency of the orthotropic compliance for Chinese fir wood [*Cunninghamia lanceolata* (Lamb.) Hook] has been investigated by performing compressive creep experiments in all orthotropic directions. Time evolution of the creep strain in the axial and lateral directions was recorded by means of the digital image correlation (DIC) technique, to determine the diagonal and nondiagonal elements of the viscoelastic compliance matrix. The results reveal the significant influence of time on the mechanical behavior. The orthotropic nature of the viscoelastic compliance is highlighted by the different time dependency of the Young's moduli and the Poisson's ratios obtained for the individual directions. Differences among the time-dependent stress-strain relationship determined at the 25, 50, and 75% stress levels indicate that the viscoelastic behavior of wood is also load-dependent. A Poisson's ratio values, which are increasing with time in ν_{LR}, ν_{LT}, ν_{RT}, ν_{TR}, and decreasing in ν_{RL} and ν_{TL}, demonstrate that the creep strain is influenced by loading directions. The substantially different time dependency of the nondiagonal elements of the compliance matrix further reveals the orthotropic compliance asymmetry and emphasizes the complexity of the viscoelastic character of wood.

Keywords: axial strain, Chinese fir wood, compressive creep test, lateral strain, orthotropic viscoelasticity, Poisson's ratios, stress level, time dependence, Young's moduli

***Corresponding author: Jiali Jiang,** State Key Laboratory of Tree Genetics and Breeding, Research Institute of Wood Industry, Chinese Academy of Forestry, Beijing 100091, P. R. China; and Institute for Building Materials, ETH Zurich, 8093 Zurich, Switzerland, e-mail: jialiwood@caf.ac.cn
Bachtiar Erik Valentine and Peter Niemz: Institute for Building Materials, ETH Zurich, 8093 Zurich, Switzerland
Jianxiong Lu: State Key Laboratory of Tree Genetics and Breeding, Research Institute of Wood Industry, Chinese Academy of Forestry, Beijing 100091, P. R. China

Introduction

Wood cell wall can be regarded as a two phase composite of elastic highly organized fibrils of cellulose surrounded by an amorphous and viscoelastic lignin-hemicellulose matrix. This implies that its mechanical behavior depends on both elastic and viscous (time-dependent) properties (Schniewind and Barrett 1972; Lakes 2009). Wood is an orthotropic and anisotropic material and its viscoelastic properties are significantly influenced by grain orientations (Backman and Lindberg 2001; Mano 2002; Jiang and Lu 2009; Ozyhar et al. 2013a). For a numerical simulation of the time-dependent behavior of wood, viscoelastic properties have to be known. Numerous investigations have been carried out by considering the time-dependent characteristics of wood and wood composites (Dlouha et al. 2009; Engelund and Svensson 2011; Engelund and Salmén 2012; Chang et al. 2013; Violaine et al. 2015). Numerical implementations that take into account the anisotropic viscoelastic nature of wood were also addressed (Hanhijärvi 1995; Schmidt and Kaliske 2004; Vidal-Sallé and Chassagne 2007; Taniguchi et al. 2010; Hassani et al. 2015). Viscoelastic material properties are generally determined either in creep or in stress relaxation experiments. In the present paper the focus is on the creep behavior.

According to Hunt (1999), wood creep has three components, which can be influential at the same time: (1) Pure viscoelastic component (time-dependent creep), is a time-dependent function of the material under constant environmental conditions; (2) the mechano-sorptive creep, which is associated with transient moisture content (MC) changes under mechanical loading (Grossman 1976); (3) pseudo creep and recovery phenomenon, which is manifested during continued moisture cycling and it becomes visible in the increased creep deflection during desorption and decreased deflection during adsorption. Though interaction among these components complicates the situation, the individual components has to be characterized to understand the time-dependent creep effects (Ozyhar et al. 2013a).

A lot of investigations concentrated on the experimental determination and analytical expressions of the mechano-sorptive creep (Mukudai and Yata 1988; Hunt 1989; Toratti and Svensson 2000; Navi et al. 2002; Takahashi et al. 2004, 2005, 2006; Dong et al. 2010; Kaboorani et al. 2013; Violaine et al. 2015). However, the pure viscoelastic creep is usually neglected in numerical models and received much less attention compared to the mechano-sorptive effects (Liu 1993). This component, however, is needed not only for a full description of the time-dependent material behavior under constant climatic conditions, but also for the determination of the components concerning the mechano-sorption, the pseudo creep, and recovery (Hering and Niemz 2012).

According to Ozyhar et al. (2013a), the determination of the pure viscoelastic component is especially time consuming. The separation of the pure viscoelastic and mechano-sorptive creep component is difficult and the experiments with this regard have to be performed under strictly constant environmental conditions. Even small fluctuations in MC lead to a merging of the two components and aggravate a clear analysis. The pure viscoelastic creep component were analyzed by Schniewind and Barrett (1972), Hayashi et al. (1993), and Taniguchi et al. (2010). Only a few studies focused on selected time-dependent parameters. The elastic properties are presented as a full compliance matrix (Bucur and Archer 1984; Keunecke et al. 2008; Hering et al. 2012; Ozyhar et al. 2012, 2013b,c), but the viscoelastic characterization of the orthotropic compliance, including the time functions for all compliance parameters, is only attempted by Ozyhar et al. (2013a). Generally, the lack of knowledge of the time-dependent behavior of the Poisson's ratios particularly inhibits the determination of the nondiagonal elements of the viscoelastic compliance matrix of wood. Some reports proved experimentally that Poisson's ratios are time dependent (Schniewind and Barrett 1972; Taniguchi and Ando 2010; Taniguchi et al. 2010), but many contradictory results caused confusion with this regard.

The intention of the present study is to investigate the time-dependent pure creep behavior of wood within the framework of linear viscoelasticity. Compressive creep experiments should be performed on Chinese fir wood in all orthotropic directions at three stress levels. Time-dependent Young's moduli and Poisson's ratios will be observed by digital image correlation (DIC) as a function of time of the strain in the axial and lateral directions. By determining the viscoelastic compliance matrix, the following topics will be addressed: (1) The pure creep behavior in the three orthotropic directions; (2) The time function on the diagonal and nondiagonal elements of the viscoelastic compliance matrix, including Young's moduli and Poisson's ratios; (3) Influence of stress levels on the pure creep behavior.

Materials and methods

Chinese fir [*Cunninghamia lanceolata* (Lamb.) Hook] plantation wood was tested. The average wood density, determined at 20°C and a relative humidity (RH) of 65% amounted to 323 kg m^{-3} and the MC was 12.2%. The clear specimens were cut from the heartwood part of a same trunk. Intrinsic knots and defects were excluded.

Dog-bone shaped specimens, as displayed in Figure 1, were tested. The cuboid profile in the cross section of the specimen allows for the simultaneous measurement of lateral strains in two separate directions and is suitable to determine two Poisson's ratios on one specimen. All specimens were conditioned in climatic chambers at 20°C and 65% RH within 6 weeks until equilibrium moisture content (EMC) was reached. Specimens with the same dimensions were prepared for all orthotropic directions: *L*- longitudinal, parallel to the grain direction, *R*- radial, perpendicular to the growth rings, *T*- tangential to the growth rings. The time consuming nature of the experimental setup inhibited testing a large number of specimens: the data were obtained from a total of 27 specimens for the orthotropic directions *L*, *R*, and *T* and the stress levels of 25, 50, and 75%.

A high-contrast random dot texture ("speckle pattern"), as described in Keunecke et al. (2008), was sprayed on two adjacent sides of the waisted specimen section (11×14 mm^2, Figure 1). An airbrush gun (Harder & Steenbeck, Germany) and finely pigmented acrylic paint (Airbrush, Pro-color by NANSA, USA) was used to obtain very fine speckles with a high-resolution pattern. First, a white ground coat and then black speckles were applied, resulting in a speckle pattern of heterogeneous gray values. These patterns are needed for the evaluation

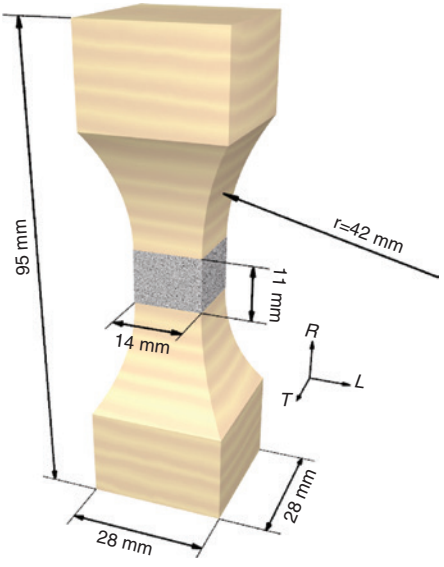

Figure 1: Dog-bone shaped specimen for creep experiments. Figure represents a specimen with a high contrast random speckle pattern and the loading axis in the *R* direction (all dimensions in mm), [Ozyhar et al. (2013a)].

of strains at the specimen surface during compression creep tests by means of the DIC software. Before creep testing, the specimens with speckle pattern were conditioned at 20°C and 65% RH for a period of 4 weeks, allowing for the equilibration of the painting effect.

The uniaxial compressive creep tests were carried out in a climatic room (20°C, 65% RH). A constant MC of the specimens was ensured by controlling the temperature and RH over the entire test duration, and the possible stress induced MC change due to coupling effects was neglected. To exclude mechano-sorptive effects, i.e. increased creep due to variations in MC during loading, experiments were performed on specimens previously preconditioned under testing conditions and reached the EMC state.

Instrument for creep experiments: Zwick Z010 testing machine (Zwick/Roell, Germany) with a 10 kN loading cell. The testing procedure consisted of the initial loading phase (displacement controlled test) and the creep phase (force controlled test under constant load). The first one was carried out with a constant loading rate of 0.05 mm min^{-1}. The resulting loading time was dependent both on the loading direction and the applied creep load level and varied between 210 and 390 s. The creep phase lasted for 24 h starting from the point when the predefined creep load was reached. The creep load applied was adjusted to the grain orientation directions. The load levels were set at 25, 50, and 75% of the yield stress (the stress at 0.2% plastic strain), respectively, for both the *R* and *T* directions. As for *L* direction, the load levels were set at 25, 50, and 75% of the ultimate stress (see Table 1).

A DIC technique (Vic-2D, Correlated Solutions, USA) was used to capture the strains during the creep experiments as suggested by Ozyhar et al. (2013a). It provides high measurement accuracy that allows for simultaneous capture of the axial and lateral strains, and therefore ensures the determination of both the Young's moduli and the time-dependent Poisson's ratios. A multiple camera system (Schneider, Germany) with a resolution of 2048×2048 pixels was applied to capture the images needed for the strain evaluation. Two cameras enabled the simultaneous measurement of the lateral strains in two directions on one specimen, which therefore allowed the determination of two corresponding Poisson's ratios from one measurement.

Images were recorded with a pair of charge coupled device (CCD) digital cameras. Snapshots were taken every 3 min over the creep experiments period, which gave a total of 480 images per camera for the creep phase and, depending on the preloading time, and additional 14–26 pictures for the loading phase (snapshots were taken every 15 s), which were required for the determination of the instantaneous Young's moduli and Poisson's ratios. The time evolution of the strains was calculated by correlating the recorded images of the deformed pattern to that in the undeformed state, i.e. the first image taken just before the start of the loading phase. Per definition, the increasing strain values correspond to the elongation, and the decreasing values to the contraction of the specimen.

Table 1: Creep load levels for Chinese fir wood in all orthotropic directions.

			Creep load (MPa)
Stress levels	**σ_L (Ultimate stress: 26.2)**	**σ_R (Yield stress: 3.0)**	**σ_T (Yield stress: 2.3)**
25%	6.5	0.8	0.6
50%	13.1	1.5	1.1
75%	19.5	2.2	1.7

L, longitudinal; *R*, radial; *T*, tangential.

Viscoelastic compliance matrix: According to Ozyhar et al. (2013a), derived from the linear viscoelastic theory, the stress-strain relationship for wood under creep at constant environmental conditions can be written as

$$\varepsilon_{\text{total}} = D_s^0 \sigma (1+\phi(t)) \tag{1}$$

Where $\varepsilon_{\text{total}}$ is the total creep strain, D_s^0 is the steady-state elastic compliance, σ is the stress and $\phi(t)$ is the time-dependent relative creep function expressed by the quotient of the creep $\varepsilon_c(t)$ and the elastic ε_{el} strain is

$$\phi(t) = \frac{\varepsilon_c(t)}{\varepsilon_{el}} = \frac{D_c(1-e^{-\frac{t}{\lambda}})}{D_s^0} \tag{2}$$

Where D_c is the creep compliance, λ is the delay time.

Based on the orthotropic material behavior assumed for wood (Bodig and Jayne 1982), the D_s^0 written in the matrix form becomes

$$D_s^0 = \begin{bmatrix} d_{11} & d_{12} & d_{13} & 0 & 0 & 0 \\ d_{12} & d_{22} & d_{23} & 0 & 0 & 0 \\ d_{13} & d_{23} & d_{33} & 0 & 0 & 0 \\ 0 & 0 & 0 & d_{44} & 0 & 0 \\ 0 & 0 & 0 & 0 & d_{55} & 0 \\ 0 & 0 & 0 & 0 & 0 & d_{66} \end{bmatrix} \tag{3}$$

whereby the diagonal elements d_{ii} of the compliance matrix are denoted as

$$d_{11}=E_L^{-1};\ d_{22}=E_R^{-1};\ d_{33}=E_T^{-1};\ d_{44}=G_{LR}^{-1};\ d_{55}=G_{LT}^{-1};\ d_{66}=G_{RT}^{-1} \tag{4}$$

and the nondiagonal elements d_{ij} ($i \neq j$) as

$$d_{12}=-\nu_{LR}\cdot d_{22};\ d_{21}=-\nu_{RL}\cdot d_{11};\ d_{13}=-\nu_{LT}\cdot d_{33};\ d_{31}=-\nu_{TL}\cdot d_{11};\ d_{23}=-\nu_{RT}\cdot d_{33};\ d_{32}=-\nu_{TR}\cdot d_{22} \tag{5}$$

where E, ν, and G are for the Young's modulus, the Poisson's ratio, and the shear modulus, respectively. The lower case indices indicate the *L*, *R*, and *T* directions, respectively. The symbols *L-R*, *L-T*, *R-T*, *R-L*, *T-R* and *T-L* are for the corresponding planes.

The creep behavior can be expressed according to Ormarsson et al. (2010) by the creep compliance matrix D_c

$$D_c(t) = \begin{bmatrix} E_L^{-1}\phi_L(t) & -E_R^{-1}\nu_{LR}\phi_{LR}(t) & -E_T^{-1}\nu_{LT}\phi_{LT}(t) & 0 & 0 & 0 \\ -E_L^{-1}\nu_{RL}\phi_{RL}(t) & E_R^{-1}\phi_R(t) & -E_T^{-1}\nu_{RT}\phi_{RT}(t) & 0 & 0 & 0 \\ -E_T^{-1}\nu_{TL}\phi_{TL}(t) & -E_R^{-1}\nu_{TR}\phi_{TR}(t) & E_T^{-1}\phi_T(t) & 0 & 0 & 0 \\ 0 & 0 & 0 & G_{LR}^{-1}\phi_{LR}(t) & 0 & 0 \\ 0 & 0 & 0 & 0 & G_{LT}^{-1}\phi_{LT}(t) & 0 \\ 0 & 0 & 0 & 0 & 0 & G_{RT}^{-1}\phi_{RT}(t) \end{bmatrix} \tag{6}$$

The instantaneous Young's moduli E_i were defined by the effective modulus obtained from the ratio of the change in stress $\Delta\sigma$ to the strain-change $\Delta\varepsilon$ determined from the stress-strain diagram in the loading phase

$$E_i(t)=E_i(t_0)=\frac{\Delta\sigma_i}{\Delta\varepsilon_i},\ i\in R,L,T \text{ with } t\le t_0 \tag{7}$$

where t_0 is the end of loading phase and the beginning of creep phase.

The instantaneous Poisson's ratios, given by the negative ratio of the passive (lateral) strain ε_i to the active (axial) strain ε_j at the time t_0, which were determined from the linear regression of the passive-active strain diagram in the linear elastic range, by simultaneous measuring the strain in the axial and lateral directions during the loading phase:

$$\nu_{ij}(t)=\nu_{ij}(t_0)=-\frac{\varepsilon_i}{\varepsilon_j},\ i\in R,L,T \text{ and } i\neq j \text{ with } t\le t_0 \tag{8}$$

The time-dependent Young's modulus $E_i(t)$ was obtained from the time evolution of the creep strain in the loading direction $\varepsilon_i(t)$ and the creep stress σ_i given in Table 1.

$$E_i(t)=\frac{\sigma_i}{\varepsilon_i(t)} \text{ with } t>t_0 \tag{9}$$

The time-dependent Poisson's ratios $\nu_{ij}(t)$ were determined by measuring the strain in the axial and lateral directions as a function of time

$$\nu_{ij}(t)=-\frac{\varepsilon_i(t)}{\varepsilon_j(t)} \text{ with } t>t_0 \tag{10}$$

In order to compare the time effect on the different Young's moduli and Poisson's ratios, the experimental values for $E(t)$ and $\nu(t)$ determined on varying specimens were normalised according to

$$\tilde{E}(t)=\frac{E(t)}{E(t_0)},\ \tilde{\nu}(t)=\frac{\nu(t)}{\nu(t_0)} \tag{11}$$

Results and discussion

Time-dependent of the orthotropic Young's moduli

Table 2 summarises the instantaneous Young's modulus $E(t_0)$ and the values determined after 24 h creep test $E(t_{24})$ for the individual orthotropic directions at three stress levels. The variability of results was calculated based on the coefficient of variation (COV) obtained from the average of three specimens for each test conditions. The relatively higher values of error are due to the high natural variability of the mechanical properties of wood (Bodig and Jayne 1982).

To compare the time evolution of the Young's moduli within and between the individual orthotropic directions and the values obtained at three stress levels, the time-dependent moduli $E(t)$ were normalised according to Eq. (11). The results show that Young's moduli exhibit a decreasing trend with time and that the creep behavior highly depends on the orthotropic direction and stress levels (Figure 2). The normalised Young's moduli $\tilde{E}(t)$ (clearly reveals that data in the R and T directions (E_R, E_T) are decreasing with time to a significantly higher extent than those in the L direction E_L. $\tilde{E}_R(t)$ is more affected than $\tilde{E}_T(t)$. Tracheids orientation in the L direction is the reason for higher E_L data, and in the case of E_R and E_T the data are proportional to the density (Keunecke et al. 2007; Gonçalves et al. 2011). Consequently, Chinese fir wood with its low density shows a tendency to smaller R and T stiffnesses and, therefore, larger differences are seen between $\tilde{E}(t)$ in longitudinal and transverse directions. One should keep in mind that in the dog-bone shaped samples of the Chinese fir wood the earlywood region within a growth ring was large, which was probably leading to the lower Young's moduli in R direction than that in T direction. Figure 2 also reveals that the time effect highly depends on the stress level in all directions. Increasing loading level deteriorated the Young's moduli, which decreased with time. The $E_R(t)$ and $E_T(t)$ data indicate that the moduli determined at 75% stress level are affected by the time by about twice as much as the moduli obtained at the 25% stress level. A similar trend applies for the $E_L(t)$, even though not as pronounced as in the R and T directions. The observed differences with this regard are corroborated by the different time evolution of the axial strain (Figure 3). The higher the stress level, the larger axial strain is found in all directions.

Time-dependent of the Poisson's ratio

Table 2 summarises the instantaneous Poisson's ratios $\nu(t_0)$ and the values determined after 24 h creep test $\nu(t_{24})$ for the individual orthotropic planes. Similar to the Young's moduli, there is a relatively high data scatter, which is especially striking for the ν_{RL} and ν_{TL}, and which is attributable to the high natural variability of wood. A similar high variability of the Poisson's ratios was observed for European beech wood (Hering et al. 2012; Ozyhar et al. 2012, 2013a). The results presented in Table 2 also indicate that the data are independent of the stress level.

The normalized Poisson's ratios $\tilde{\nu}(t)$ are also time dependent and this behavior strongly influenced by the orthotropic direction and load level (Figure 4). The Poisson's ratios of L-loaded specimens (ν_{RL} and ν_{TL}) are affected by time to a much higher extent than those loaded in R

Table 2: Time dependency of the Young's moduli and Poisson's ratios for Chinese fir wood in all orthotropic directions.

Stress level		Young' moduli (MPa)				Poisson's ratios (-)					
		E_L	E_R	E_T		ν_{RL}	ν_{TL}	ν_{LR}	ν_{TR}	ν_{LT}	ν_{RT}
25%	$E(t_0)$	6319 (14.6)	465 (17.6)	257 (13.4)	$\nu(t_0)$	0.13 (15.4)	0.17 (19.6)	0.05 (14.8)	0.78 (22.3)	0.08 (17.8)	0.82 (10.4)
	$E(t_{24})$	5996 (16.5)	404 (12.0)	244 (7.2)	$\nu(t_{24})$	-0.04 (16.3)	-0.27 (21.1)	0.07 (21.2)	0.92 (17.3)	0.09 (15.5)	0.87 (27.1)
50%	$E(t_0)$	6145 (12.8)	437 (10.2)	268 (11.1)	$\nu(t_0)$	0.11 (28.2)	0.20 (19.3)	0.04 (23.3)	0.38 (12.4)	0.07 (16.9)	0.70 (18.1)
	$E(t_{24})$	5739 (10.4)	359 (7.8)	212 (14.4)	$\nu(t_{24})$	-0.05 (12.3)	-0.34 (19.5)	0.06 (17.4)	0.47 (14.2)	0.08 (19.8)	0.75 (17.3)
75%	$E(t_0)$	5922 (14.0)	478 (11.3)	270 (6.9)	$\nu(t_0)$	0.10 (19.3)	0.19 (13.2)	0.09 (19.2)	0.81 (18.5)	0.05 (18.7)	0.65 (17.1)
	$E(t_{24})$	5500 (15.2)	387 (9.8)	237 (9.1)	$\nu(t_{24})$	-0.24 (20.4)	-0.33 (17.3)	0.10 (24.5)	0.87 (23.8)	0.08 (12.4)	0.91 (23.7)

$E(t_0)$, mean value of the instantaneous Young's modulus; $E(t_{24})$, mean value of the time-dependent Young's modulus determined after 24 h creep test; $\nu(t_0)$, mean value of the instantaneous Poisson's ratios; $\nu(t_{24})$, mean value of the time-dependent Poisson's ratios determined after 24 h creep test; *L*, longitudinal; *R*, radial; *T*, tangential; Values in parenthesis are COV.

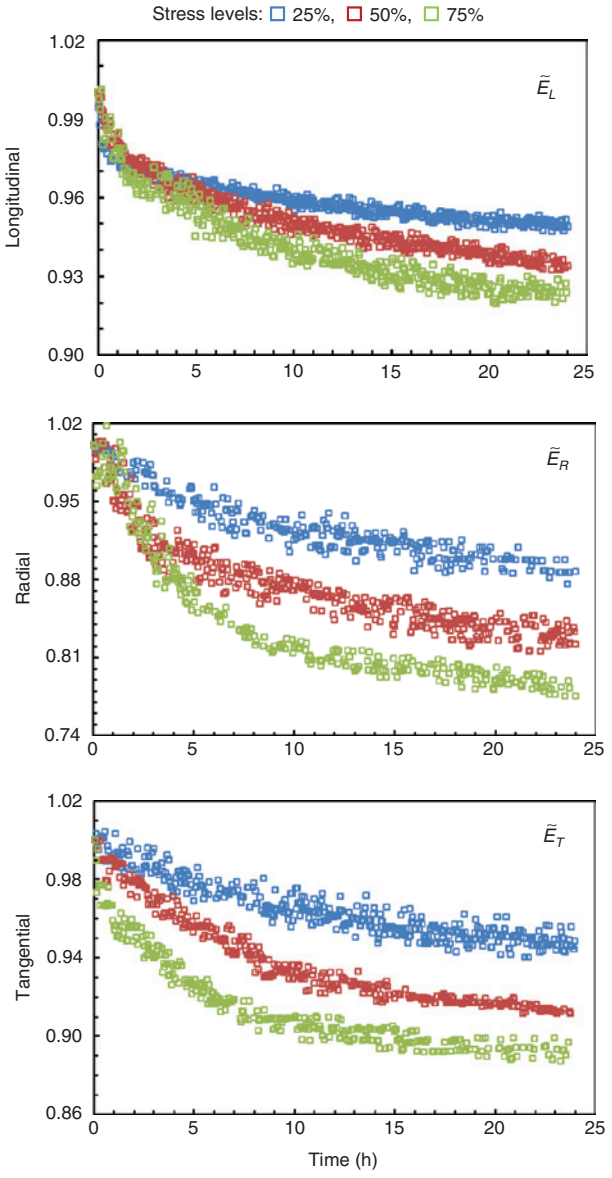

Figure 2: Time evolution of the normalized Young's moduli $\tilde{E}(t)$ for Chinese fir wood determined in compressive creep experiment at three stress levels in the indicated orthotropic directions.

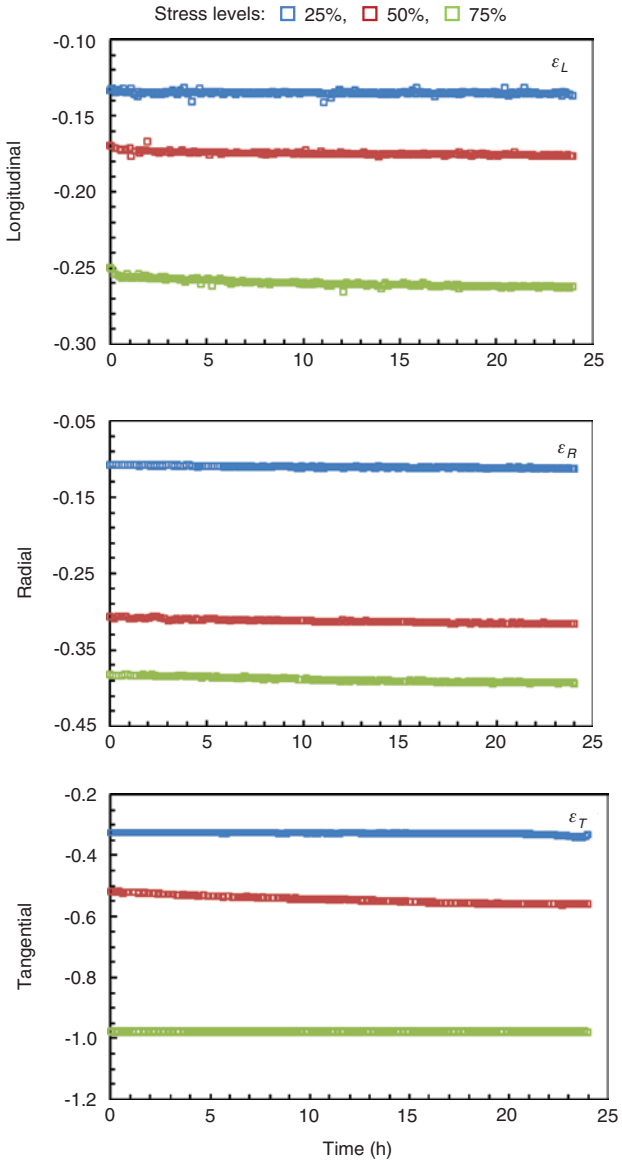

Figure 3: Time evolution of the axial strain (%) for Chinese fir wood determined in compressive creep experiment at three stress levels in the indicated orthotropic directions.

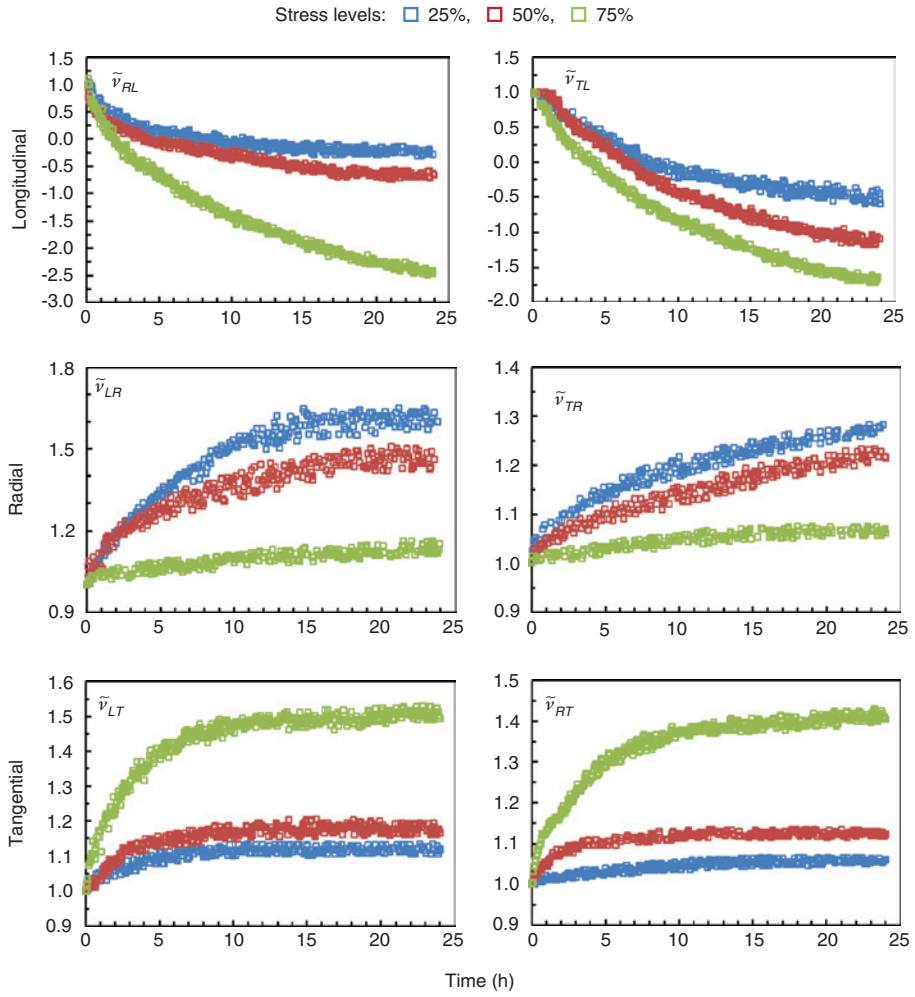

Figure 4: Time evolution of the normalised Poisson's ratio $\tilde{\nu}(t)$ for Chinese fir wood determined in compressive creep experiment at three stress levels in all orthotropic direction.

(ν_{LR} and ν_{TR}) and T (ν_{LT} and ν_{RT}) directions. Accordingly, the time-dependent behavior for Poisson's ratios with equal loading, but different direction of lateral expansion, as for the ν_{RL} and ν_{TL}, ν_{LR} and ν_{TR}, ν_{LT} and ν_{RT}, is very similar. In Figure 4, the $\tilde{\nu}(t)$ for the ν_{LR}, ν_{TR}, ν_{LT} and ν_{RT}, can be interpreted that the Poisson's ratios might be divided into an initial time-dependent stage with rapid change of Poisson's ratio and a second time insensitive stage, where the data are nearly stable after a certain time. Ozyhar et al. (2013a) reported similar results.

The comparison of the $\tilde{\nu}(t)$ values determined after 24 h of the creep further reveal that the time effect on the Poisson's ratios at 75% stress level is roughly twice as much as at 25% stress level for ν_{RL}, ν_{TL}, ν_{LT} and ν_{RT}, while ν_{LR} and ν_{TR} and present an opposite trend (Figure 4). Moreover, Poisson's ratios determined in L direction ($\tilde{\nu}_{RL}$ and $\tilde{\nu}_{TL}$), in general, are decreasing, while those obtained in R and T directions ($\tilde{\nu}_{LR}$, $\tilde{\nu}_{TR}$, $\tilde{\nu}_{LT}$ and $\tilde{\nu}_{RT}$) are increasing with time. Ozyhar et al. (2013a) reported that the overall orthotropic time-dependent behavior of the Poisson's ratios are decreasing. These inconsistent results cannot be interpreted satisfactorily. Lakes (1992) found that Poisson's ratios can increase or decrease with time, which was confirmed by Lakes and Wineman (2006): "*viscoelastic Poisson's ratios need not to increase with time, and need not to be monotonic with time*".

Figure 5 illustrates different time dependency of the lateral strain in all directions at three load levels. The time evolution of the strain show in R and T directions the expected scenario, where the contraction of the specimen in the axial direction is accompanied by the expansion in the transverse direction, and exhibit increasing trends for lateral strain data. However, the time evolution of the lateral strain in L direction reveals an opposite trend, i.e. an increasing contraction of the lateral strain instead of expansion in the R and T directions. Ozyhar et al. (2013a) found a similar trend. Although the mechanism behind this behavior are not yet completely understood,

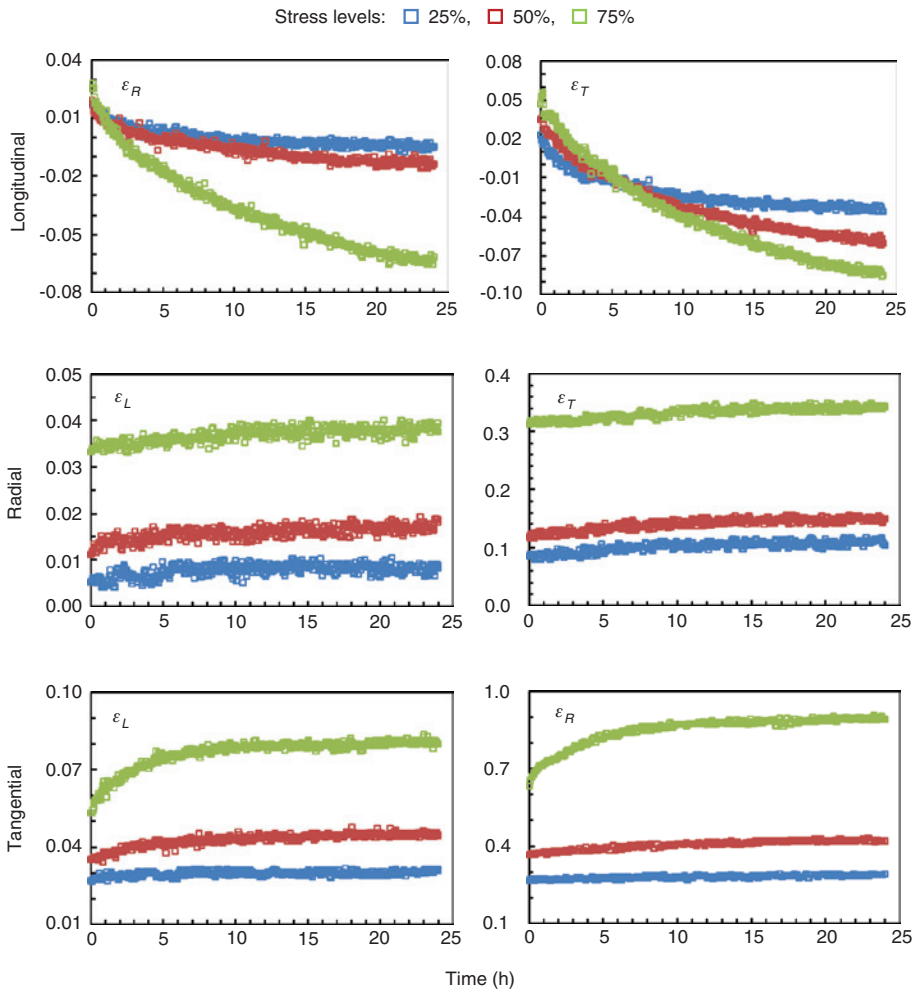

Figure 5: Time evolution of the lateral strain (%) for Chinese fir wood determined in compressive creep experiment at three stress levels in the indicated orthotropic directions.

the implications on the time-dependent behavior of the values of ν_{RL} and ν_{TL} are significant, while the data are continuously decreasing with time and reach eventually negative values (Table 3). Such negative values were also observed by Ozyhar et al. (2013a). According to Ting and Chen (2005), anisotropic elastic materials can have an arbitrarily large positive or negative Poisson's ratio values. Hilton (2009) reported that the linear viscoelastic Poisson's ratios are not limited to the elastic value range and may exceed it considerably in either direction. Negative Poisson's ratios for auxetic materials, and viscoelastic Poisson's ratios with negative values were discussed by Lakes (1987) and Lakes and Wineman (2006), respectively. A review on this phenomenon is given by Liu (2006).

According to Lakes (1993), negative Poisson's ratios can be due to the structural hierarchy of the material. It is at least conceivable that the complex wood structure is responsible to a different stress-strain response in the orthotropic directions and at different load levels (as

Table 3: Time dependency of the orthotropic compliance matrix elements for Chinese fir wood determined in compressive creep experiment.

	25% Stress		50% Stress		75% Stress	
Compliance	$d(t_0)$	$d(t_{24})$	$d(t_0)$	$d(t_{24})$	$d(t_0)$	$d(t_{24})$
d_{11}	158	167	163	174	169	182
d_{22}	215	248	229	279	209	258
d_{33}	389	410	373	472	370	422
$-d_{12}$	11	17	9	17	19	26
$-d_{21}$	21	-7	18	-9	17	-44
$-d_{13}$	31	37	26	38	19	34
$-d_{31}$	27	-45	33	-59	32	-60
$-d_{23}$	319	357	261	354	241	384
$-d_{32}$	168	228	87	131	169	224

All data in ($\times 10^{-12}$ Pa^{-1}); d, elements of the orthotropic compliance matrix (d_{ii}, diagonal; d_{ij}, nondiagonal); $d(t_0)$, instantaneous values [calculated by the Eqs. (4) and (5) with the average $E(t_0)$ and $\nu(t_0)$ values from Table 2]; $d(t_{24})$, time-dependent value determined after 24 h compressive creep test.

showed in Figures 3 and 5), and eventually to negative values of Poisson's ratio. The cellular structure of wood, which resembles that of an engineered honeycomb structure (Gibson 2005), also raises the question of whether negative Poisson's ratios could be associated with the mechanical behavior of wood at the cellular level. Compressive load applied on the wavy structure of the honeycomb cell walls, bending may occur, which causes elastic buckling and gives rise to negative Poisson's ratios. The microporous structure of wood might lead to elastic instabilities, which have been reported to explain negative Poisson's ratios in porous elastomeric materials (Bertoldi et al. 2010). Thus the negative Poisson's ratios might be attributed to several interacting mechanical processes taking place at the microscopic level (Ozyhar et al. 2013a).

Time-dependency of the orthotropic compliance matrix

The time dependency of the compressive orthotropic creep compliance elements are presented in Table 3. Accordingly, the compliance is a function of time, indicating that individual elements of the orthotropic compliance matrix are affected differently by time. Obviously, the higher the stress level, the much more time sensitive behavior can be seen. A lot of studies have pointed out that there are significant discrepancies between the corresponding values for the nondiagonal elements (d_{ij} and d_{ji}) of the wood compliance matrix (Bodig and Jayne 1982; Neuhaus 1983; Hering et al. 2012; Ozyhar et al. 2013a), even though, for simplicity reasons, these values are often assumed as equal based on the orthotropic symmetry of the compliance. However, the results in this study also indicate that the orthotropic compliance shows an asymmetric behavior.

Conclusion

The time dependency of the Young's moduli and Poisson's ratios for Chinese fir wood were determined by compressive creep tests at three stress levels. The results show that these properties are a function of time and differ in all orthotropic directions. Thus the viscoelastic behavior of wood is complex and also dependent of the loading level. Proved by the time evolution of the stress-strain relationship, the $E(t)$ and $\nu(t)$ data confirm that not only the magnitude of the time effect but also the time evolution of the behavior itself is dependent on the orthotropic directions and on the stress level. Negative Poisson's ratio values obtained for specimens compressed in the L direction (ν_{RL} and ν_{TL}) further exemplify the complexity of the viscoelastic behavior. The mechanism behind the time-dependent behavior of the negative Poisson's ratios are not completely understood yet, but the reasons for this are assumed to be closely associated with the hierarchical structure of wood and the mechanical response of wood at the cellular level. The time dependency of the orthotropic compliance asymmetry is revealed by the time evolution of the corresponding nondiagonal elements of the orthotropic compliance matrix.

Acknowledgments: This research was sponsored by the National Natural Science Foundation of China (No. 31570548). J.J. would like to gratefully acknowledge the financial support from the China Scholarship Council (CSC). A special thanks goes to Franco Michel and Thomas Schnider for their help during specimen preparation and their expert assistance in conducting the measurements.

References

Backman, A.C., Lindberg, K.A.H. (2001) Difference in wood material responses for radial and tangential direction as measured by dynamic mechanical thermal analysis. J. Mater. Sci. 36:3777–3783.

Bertoldi, K., Reis, P.M., Willshaw, S., Mullin, T. (2010) Negative Poisson's ratio behavior induced by an elastic instability. Adv. Mater. 22:361–366.

Bodig, J., Jayne, B.A. Mechanics of Wood and Wood Composites. Van Nostrand Reinhold Company Inc., New York, 1982.

Bucur, V., Archer, R.R. (1984) Elastic constants for wood by an ultrasonic method. Wood Sci. Technol. 18:255–265.

Chang, F.C., Lam, F., Kadla, J.F. (2013) Using master curves based on time–temperature superposition principle to predict creep strains of wood–plastic composites. Wood Sci. Technol. 47:571–584.

Dlouha, J., Clair, B., Arnould, O., Horáček, P., Gril, J. (2009) On the time-temperature equivalency in green wood: characterisation of viscoelastic properties in longitudinal direction. Holzforschung 63:327–333.

Dong, F., Olsson, A.M., Salmén, L. (2010) Fibre morphological effects on mechano-sorptive creep. Wood Sci. Technol. 44:475–483.

Engelund, E.T., Svensson, S. (2011) Modelling time-dependent mechanical behaviour of softwood using deformation kinetics. Holzforschung 65:231–237.

Engelund, E.T., Salmén, L. (2012) Tensile creep and recovery of Norway spruce influenced by temperature and moisture. Holzforschung 66:959–965.

Gibson, L.J. (2005) Biomechanics of cellular solids. J. Biomech. 38:377–399.

Gonçalves, R., Trinca, A.J., Cerri, D.GP. (2011) Comparison of elastic constants of wood determined by ultrasonic wave propagation and static compression testing. Wood Fiber Sci. 43:64–75.

Grossman, P.U.A. (1976) Requirements for a model that exhibits mechano-sorptive behavior. Wood Sci. Technol. 10:163–168.
Hanhijärvi, A. (1995) Modelling of creep deformation mechanisms in wood. Technical Research Centre of Finland, 79–91.
Hassani, M.M., Wittel, F.K., Hering, S., Herrmann, H.J. (2015) Rheological model for wood. Comput. Method. Appl. Mech. Eng. 283:1032–1060.
Hayashi, K., Felix, B., Le Govic, C. (1993) Wood viscoelastic compliance determination with special attention to measurement problems. Mater. Struct. 26:370–376.
Hering, S., Niemz, P. (2012) Moisture-dependent, viscoelastic creep of European beech wood in longitudinal direction. Eur. J. Wood Wood Prod. 70:667–670.
Hering, S., Keunecke, D., Niemz, P. (2012) Moisture-dependent orthotropic elasticity of beech wood. Wood Sci. Technol. 46:927–938.
Hilton, H.H. (2009) The elusive and fickle viscoelastic Poisson's ratio and its relation to elastic-viscoelastic correspondence principle. J. Mech. Mater. Struct. 4:1341–1364.
Hunt, D.G. (1989) Linearity and non-linearity in mechano-sorptive creep of softwood in compression and bending. Wood Sci. Technol. 23:323–333.
Hunt, D.G. (1999) A unified approach to creep of wood. Proc. R. Soc. A. 455:4077–4095.
Jiang, J.L., Lu, J.X. (2009) Anisotropic characteristics of wood dynamic viscoelastic properties. Forest Prod. J. 59:59–64.
Kaboorani, A., Blanchet, P., Laghdir, A. (2013) A rapid method to assess viscoelastic and mechanosorptive creep in wood. Wood Fiber Sci. 45:370–382.
Keunecke, D., Sonderegger, W., Pereteanu, K., Lüthi, T., Niemz, P. (2007) Determination of Young's and shear moduli of common yew and Norway spruce by means of ultrasonic waves. Wood Sci. Technol. 41:309–327.
Keunecke, D., Hering, S., Niemz, P. (2008) Three-dimensional elastic behavior of common yew and Norway spruce. Wood Sci. Technol. 42:633–647.
Lakes, R.S. (1987) Foam structures with a negative Poisson's ratio. Science 235:1038–1040.
Lakes, R.S. (1992) The time-dependent Poisson's ratio of viscoelastic materials can increase or decrease. Cell. Polym. 11:466–469.
Lakes, R.S. (1993) Materials with structural hierarchy. Nature 361:511–515.
Lakes, R.S., Wineman, A. (2006) On Poisson's ratios in linearly viscoelastic solids. J. Elasticity 85:45–63.
Lakes, R.S. (2009) Viscoelastic Materials. Cambridge University Press, New York.
Liu, T. (1993) Creep of wood under a large span of loads in constant and varying environments. Part 1: experimental observations and analysis. Holz Roh- Werk. 51:400–405.
Liu, Q. (2006) Literature review: Materials with negative Poisson's ratios and potential applications to aerospace and defense. Air vehicles division, DSTO defense science and technology organization, Victoria, Australia.
Mano, F. (2002) The viscoelastic properties of cork. J. Mater. Sci. 37:257–263.
Mukudai, J., Yata, S. (1988) Verification of Mukudai's mechano-sorptive model. Wood Sci. Technol. 22:43–58.
Navi, P., Pittet, V., Plummer, C.J.G. (2002) Transient moisture effects on wood creep. Wood Sci. Technol. 36:447–462.
Neuhaus, H. (1983) Elastic behavior of spruce wood as a function of moisture content. Holz Roh- Werk. 41:21–25.
Ormarsson, S., Dahlblom, O., Johansson, M. (2010) Numerical study of how creep and progressive stiffening affect the growth stress formation in trees. Trees 24:105–115.
Ozyhar, T., Hering, S., Niemz, P. (2012) Moisture-dependent elastic and strength anisotropy of European beech wood in tension. J. Mater. Sci. 47:6141–6150.
Ozyhar, T., Hering, S., Niemz, P. (2013a) Viscoelastic characterization of wood: Time dependence of the orthotropic compliance in tension and compression. J. Rheol. 57:699–717.
Ozyhar, T., Hering, S., Niemz, P. (2013b) Moisture-dependent orthotropic tension-compression asymmetry of wood. Holzforschung 67:395–404.
Ozyhar, T., Hering, S., Sanabria, S.J., Niemz, P. (2013c) Determining moisture-dependent elastic characteristics of beech wood by means of ultrasonic waves. Wood Sci. Technol. 47:329–341.
Schniewind, A.P., Barrett, J.D. (1972) Wood as a linear orthotropic viscoelastic material. Wood Sci. Technol. 6:43–57.
Schmidt, J., Kaliske, M. (2004) Anisotropic moisture depending viscoelastic material model for wood. Proc. Appl. Math. Mech. 4:205–206.
Takahashi, C., Ishimaru, Y., Iida, I., Furuta, Y. (2004) The creep of wood destabilized by change in moisture content. Part 1: the creep behaviors of wood during and immediately after drying. Holzforschung 58:261–267.
Takahashi, C., Ishimaru, Y., Iida, I., Furuta, Y. (2005) The creep of wood destabilized by change in moisture content. Part 2: the creep behaviors of wood during and immediately after adsorption. Holzforschung 59:46–53.
Takahashi, C., Ishimaru, Y., Iida, I., Furuta, Y. (2006) The creep of wood destabilized by change in moisture content. Part 3: The influence of changing moisture history on creep behavior. Holzforschung 60:299–303.
Taniguchi, Y., Ando, K. (2010) Time-dependence of Poisson's effect in wood I: the lateral strain behavior. J. Wood Sci. 56:100–106.
Taniguchi, Y., Ando, K., Yamamoto, H. (2010) Determination of three-dimensional viscoelastic compliance in wood by tensile creep test. J. Wood Sci. 56:82–84.
Ting, T.C.T., Chen, T. (2005) Poisson's ratio for anisotropic elastic materials can have no bounds. Q. J. Mech. Appl. Math. 58:73–82.
Toratti, T., Svensson, S. (2000) Mechano-sorptive experiments perpendicular to grain under tensile and compressive loads. Wood Sci. Technol. 34:317–326.
Vidal-Sallé, E., Chassagne, P. (2007) Constitutive equations for orthotropic nonlinear viscoelastic behavior using a generalized Maxwell model application to wood material. Mech. Time-Depend. Mater. 11:127–142.
Violaine, G.R., Cisse, O., Placet, V., Johnny, B., Miguel, P., Boubakar, M.L. (2015) Creep behaviour of single hemp fibres. Part II: Influence of loading level, moisture content and moisture variation. J. Mater. Sci. 50:2061–2072.